

Magnetic resonance of plasmonic modulation and switchable routing in gated graphene waveguides and their robustness and broadband tunability

Kum-Dong Kim, Song-Jin Im ^{*}, Kil-Song Song, Ji-Song Pae, Chol-Song Ri, Kum-Song Ho, and Yong-Ha Han

Department of Physics, Kim Il Sung University, Taesong District, 02-381-4410 Pyongyang, Democratic People's Republic of Korea



(Received 2 May 2022; revised 13 June 2022; accepted 22 June 2022; published 5 July 2022)

We analytically derived an explicit condition for high-contrast plasmonic modulation and switchable routing in coupled graphene waveguides consisting of two coupled gated graphene sheets sandwiching a gyrotropic medium. The analytical condition intuitively predicts that by manipulating the graphene chemical potential and the gyration of the in-between medium we can combine robustness of the plasmonic routing to the deviation of design and material parameters due to imperfect fabrication and harsh environment with the extreme high contrast. Also, it predicts broadband tunability of the high-contrast plasmonic routing. The intuitive analytical condition reveals that the high contrast is achievable at a resonance gyration due to a magnetic resonance of nonreciprocal directional coupling. The magnetic resonance of nonreciprocity breaks a currently held preconception that the stronger magnetic field induces the stronger magnetically induced nonreciprocity. Numerical simulations demonstrate the robustness of the magnetic resonance of nonreciprocity and its tunability over a one-octave spanning spectral range. In practice, the chemical potential and the gyration can be manipulated by controlling the gate voltage of the graphene and the external magnetic field, respectively. Our findings would provide a robust and broadband tunable tool for high-contrast plasmonic modulator and switchable router and for probing of ultrafast magnetization dynamics.

DOI: [10.1103/PhysRevB.106.L041401](https://doi.org/10.1103/PhysRevB.106.L041401)

Plasmonic waveguides offer a promising route for the development of next-generation integrated nanophotonic circuits [1] and key elements of nanophotonic circuits are plasmonic modulators, controllable plasmonic splitters, and routers. Plasmonic modulators have been proposed based on diverse principles including the Pockels effect [2–4], the thermo-optical effect [5,6], and gain-assisted cavity coupling [7–9]. Whereas the combination of plasmonics with magnetism become an active topic of research to achieve new functionalities in nanosystems, the magneto-optical effect has the advantage compared with other proposed principles, such as the electro-optical effect and thermo-optical effect that the switching can be much faster [10]. The generation of magnetic fields by integrated electronic circuits can easily reach speeds in the gigahertz regime. Furthermore, the effective magnetic fields can be generated by the terahertz electromagnetic pulses [11] and optical excitation with the femtosecond laser pulse is also very promising since it can provide a spatial gradient of the effective magnetic fields on submicron scales [12–15].

The performance of compact magneto-optical modulators generally suffers from the small magneto-optical effect. A compact configuration based on a magnetoplasmonic interferometer engraved in a hybrid ferromagnetic structure was successfully developed, and its modulation contrast was on the level of 2% at a waveguide length of 20 μm [16]. The configuration using the plasmon-enhanced transverse magneto-optical Kerr effect in nanopatterned gold/garnet structures [17], being relatively bulky and not fully waveguide

integrated, was experimentally demonstrated to be resonantly sensitive to the magnetically induced changes of plasmonic wave number and allows a modulation contrast of 50%. Many other elaborate configurations have been proposed to resonantly enhance the magneto-optical effect and increase the modulation contrast at the expense of reduced bandwidth determined by the resonant configurations [18–26]. On the other hand, graphene is a new kind of plasmonic material which found wide applications, in particular, in the terahertz to mid-infrared frequency range because graphene plasmons provide an extremely tight mode confinement and a lower ohmic loss compared to those by conventional plasmonic materials, such as gold and silver and they are flexibly controllable by using the graphene's gate voltage [27–32]. The magneto-optical properties of graphene in a magnetic field directed perpendicularly to its plane were employed by graphene-based magnetoplasmonic devices [33–35]. However, they are nonsensitive to an in-plane magnetic field. Graphene-covered gyrotropic medium in the in-plane magnetic field presents interesting magnetoplasmonic effects which is promising for compact, high-quality factor, and tunable magnetoplasmonic devices [36,37]. In practice, sandwiching graphene structures [38–40] and a graphene-covered magneto-optical semiconductor film [41] have been fabricated.

In this Letter we present robust and broadband tunable plasmonic routing based on a magnetic resonance of nonreciprocal directional coupling in coupled gated graphene waveguides. So far, for most of suggested devices based on magnetically induced nonreciprocity it has been conventional that the larger gyration induces the stronger nonreciprocity. The plasmonic routing presented in this Letter has the

^{*}sj.im@ryongnamsan.edu.kp

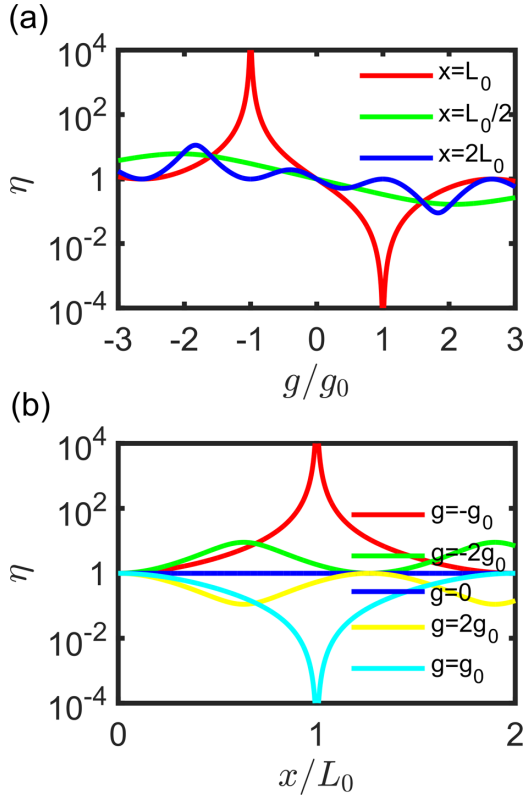


FIG. 2. Power splitting ratio according to the (a) gyration and (b) the propagation length in the coupled graphene waveguides. The results have been calculated from Eq. (5). In (a) the red, green, and blue curves are for $x = L_0$, $x = L_0/2$, and $x = 2L_0$, respectively. In (b) the red, green, blue, yellow, and cyan curves are for $g = -g_0$, $g = -2g_0$, $g = 0$, $g = 2g_0$, and $g = g_0$, respectively.

Here $\alpha = e^2/(4\pi\hbar c\epsilon_0) \approx 1/137$ is the fine-structure constant. In the derivation of Eqs. (5)–(8) we applied the first order of approximation with respect to $|(\beta^0 - \beta^e)/(\beta^0 + \beta^e)| \ll 1$, which is justified for a gap thickness between the two graphene sheets larger than the skin depth. In the derivation we disregarded i/τ of Eq. (1). Figure 2 shows results from Eqs. (5)–(7). As shown in Fig. 2(a), the power splitting ratio can be controlled by changing g/g_0 . As shown in Fig. 2(b), the power splitting ratio oscillates according to x/L_0 . In practice, the manipulation of the gyration g can be realized with an external magnetic field. From Fig. 2 we can see $\eta(g = g_0, x = L_0) = 0$ and $\eta(g = -g_0, x = L_0) = +\infty$ that imply the condition $(g = \pm g_0, x = L_0)$ for high-contrast plasmonic modulation and switchable routing. The high-contrast plasmonic modulation and switchable routing is achievable for a resonance value g_0 of the gyration. Although Eq. (5) gives general information for the power splitting ratio, and the magnetic resonance is shown in Fig. 2(a), it is difficult to anticipate the magnetic resonance directly from Eq. (5). At $x' = [2/(1 + g^2)]^{1/2}$ Eq. (5) leads to

$$\eta(x) \approx |\xi_1/\xi_2|^2 = \left| \frac{g' - 1}{g' + 1} \right|^2, \quad (9)$$

which is very intuitive for the magnetic resonance. We call g_0 the resonance gyration. In Eqs. (6)–(8), we introduced a

parameter, the plasmonic thickness of the gyrotropic layer between the two graphene sheets $2a_g = 2an_{\text{eff}}$, where $2a$ is the real thickness and n_{eff} is the effective refractive index for the plasmon as similar as the optical length is defined as the product of the length and the refractive index. The physical meaning of the plasmonic thickness is the plasmonic phase difference through the thickness divided by the vacuum wave-number k_0 . In fact, k_0a_g is a crucial parameter for determining the resonance gyration g_0 , L_0 , and the power splitting ratio η as seen in Eqs. (5)–(8). The plasmonic thickness of the gyrotropic layer $2a_g$ can be manipulated by changing the graphene chemical potential μ_c with the gate voltage of the graphene. Thus, we can predict that for arbitrary values of the deviation of design and material parameters and for a broadband range of the operation frequency the high-contrast condition ($g = \pm g_0, x = L_0$) can be satisfied by manipulating the gyration g and the chemical potential μ_c . We note that Eqs. (6)–(8) imply, intuitively, ways for changing values of the chemical potential and the gyration needed for the high-contrast plasmonic modulation and switchable routing. The resonance gyration g_0 exponentially decreases with the increase in $2k_0a_g$ which is proportional to the gap thickness among the two graphene sheets $2a$, the environmental material parameter $\epsilon_1 + \epsilon_2$, and the squared value of the operation frequency ω^2 . The needed value of the chemical potential μ_c is proportional the squared value of the operation frequency ω^2 .

Figure 3 shows the high-contrast switchable routing and its structural and environmental robustness. Figure 3(a) shows the scheme for numerical simulation. The vertical dotted line shows the interface between the no-gyration part $g = 0$ and the gyrotropic part $g = \pm g_0$. The symmetric mode (odd mode) of the no-gyration part $g = 0$ is incident to the left port. Figures 3(b)–3(e) show results of the numerical simulation for the distribution of $\text{Re}(H_y)$ in the coupled gated graphene waveguides demonstrating the switchable plasmonic routing with the extremely high contrast. Here, $g_0 = 0.12$, calculated from Eq. (6), is used for the simulation. One can see that the field intensity is concentrated on the top graphene, which is switched to the bottom graphene by altering the gyration from $g = g_0$ to $g = -g_0$. The gyration altering can be realized by the reversal of the magnetic-field direction. The graphene chemical potential μ_c calculated from Eqs. (7) and (8) has been used for the numerical simulation. Figures 3(f)–3(h) show that the extremely high contrasts more than 10^3 (99.9%) are preserved in the deviation of design and material parameters a , L , and ϵ_1 . The red curves have been obtained from Eqs. (7) and (8) predicting the chemical potential μ_c according to the a , L , and ϵ_1 for preserving the extremely high contrast. This prediction has been demonstrated by the extremely high contrasts from numerical simulations for the parameters corresponding to the blue circles on the red curves. In the numerical simulation we assumed $\tau = 1$ ps as the carrier relaxation time of graphene, which is experimentally achievable at room temperature [43]. We note that the high-contrast condition ($g = \pm g_0, L = L_0$) from Eqs. (5)–(9) disregarding i/τ well agrees with the simulation results taking into account i/τ . The absorption results in an insertion loss, however, it does not influence the high contrast because the intensity reduction due to the absorption occur equally in the both channels.

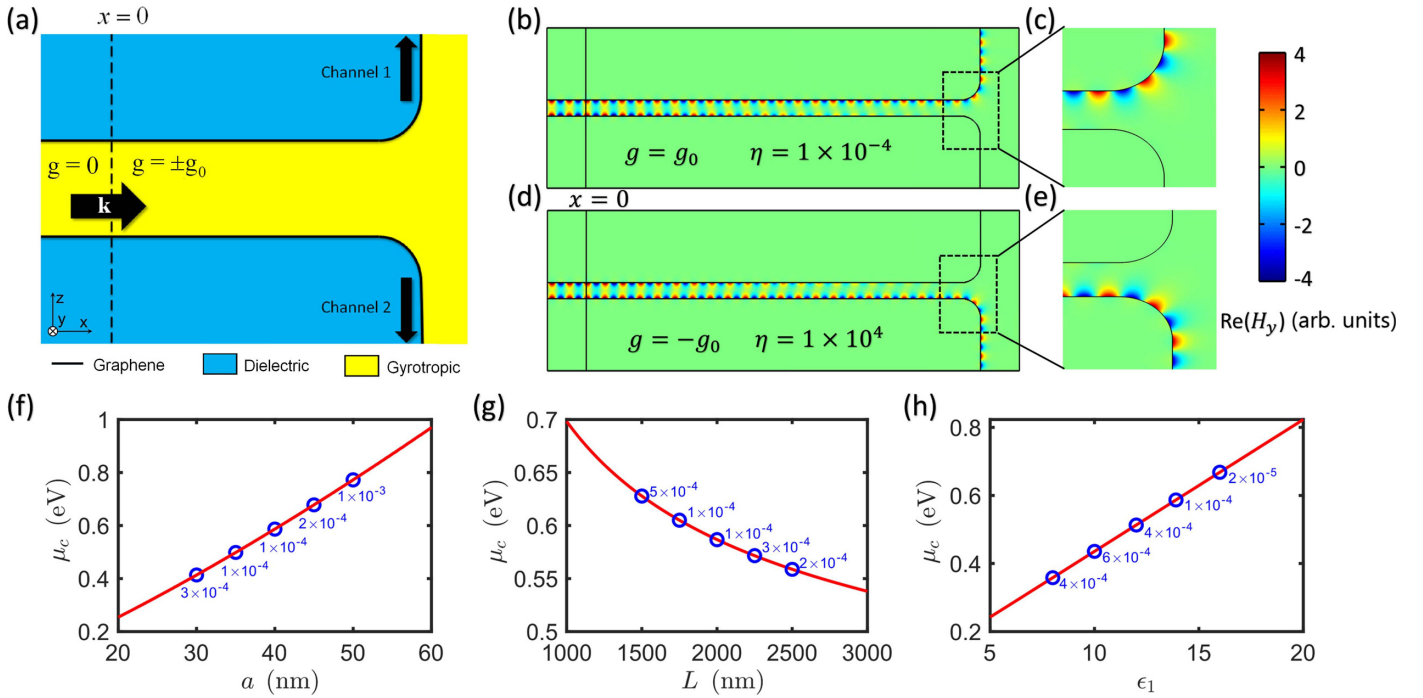


FIG. 3. Robustness of the high-contrast switchable plasmonic routing to the deviation of the design and material parameters. (a) shows the scheme of the plasmonic routing. (b)–(e) show numerical simulation results for the distribution of $Re(H_y)$ in the coupled gated graphene waveguides. In (b)–(e) the design and material parameters have been assumed to be $a = 40$, $L = 2000$ nm, $\epsilon_1 = 13.9$, and $\epsilon_2 = 1$. The gyration has been altered from $g = g_0$ [(b) and (c)] to $g = -g_0$ [(d) and (e)]. In (f)–(h) the red curves show the graphene chemical potential calculated from $L_0 = L$ and Eqs. (7) according to a , L , and ϵ_1 , respectively. Numerical simulations have been performed for the parameters at the blue circles on the red curves of in (f)–(h). Values of the power splitting ratio have been obtained from the numerical simulations and they have been shown near the blue circles. For the numerical simulations we used $g = g_0$ calculated from Eqs. (6). The operation frequency is 30 THz.

Figure 4 shows results of the numerical simulation in the coupled gated graphene waveguides demonstrating the broad-

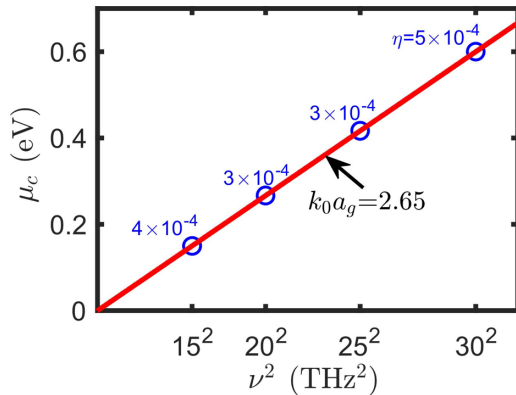


FIG. 4. Broadband tunability of the high-contrast switchable plasmonic routing over a one-octave-spanning spectral range. The design and material parameters have been assumed to be $a = 40$, $L = 1800$ nm, $\epsilon_1 = 13.9$, and $\epsilon_2 = 1$. The red straight line shows the chemical potential versus the second power of the frequency, which has been obtained from Eqs. (7) and (8). Numerical simulations have been performed for the parameters corresponding to the blue circles on the red straight line. Values of the power splitting ratio have been obtained from the numerical simulations, and they have been shown near the blue circles. For the numerical simulations we used $g = g_0$ calculated from Eqs. (6).

band tunability of the high-contrast switchable routing over a one-octave-spanning spectral range. Here, the red straight line is from Eq. (8) for $k_0 a_g = 2.65$ corresponding to the parameters $a = 40$, $L = L_0 = 1800$ nm, $\epsilon_1 = 13.9$, and $\epsilon_2 = 1$ in Eq. (7). The extremely high contrasts from the numerical simulation (the values near the blue circles on the red curve) demonstrate the linear relation between the chemical potential and the second power of the tuned frequency. The extremely high contrasts more than 10^3 (99.9%) are preserved over the one-octave-broad spectral range. We note that through the Letter we do not assume any particular dependence of the gyration on the external magnetic field and the frequency. For a magneto-optical semiconductor, if we assume that the cyclotron frequency ω_c is far smaller than the considering angular frequency ω , $g \approx \omega_{pl}^2 \omega_c / \omega^3$ where ω_{pl} is the plasma angular frequency [44]. Via the cyclotron frequency $\omega_c = eB^{ext} / m_{eff}$, where e and m_{eff} are the charge and effective mass of electrons, respectively, the gyration g can be manipulated with the external magnetic-field B^{ext} . The gyration g strongly depends on the angular frequency ω : It is reversely proportional to the third power of ω [24]. For example, a strength of the external magnetic field needed for the same value of the gyration at the frequency 15 THz is eight times smaller than that at the frequency 30 THz. In this Letter we intended to reveal analytically the intuitive condition for magnetic resonance of the plasmonic modulation and routing. The analytical condition from Eqs. (5)–(9) includes the gyration as one crucial parameter, and it does not include any particular

dependence of the gyration on the frequency. Thus, in order to reveal a principle for a more general case, here, we do not assume any particular dependence of the gyration on the frequency. Even, noticeable deterioration to the broadband tunability is not induced by the absence of assumption on frequency dependence of the gyration. First, needed values of the gyration is achievable by controlling the external magnetic field, second, the needed values of the gyration are allowed to be in experimentally achievable ranges: $g < 0.1$ by changing design parameters as shown in the intuitive analytical condition for the high-contrast plasmonic routing.

We investigated controllable plasmonic splitting in a coupled graphene waveguide structure. The power splitting ratio is controlled by changing the gyration of the in-between material, and a high-contrast plasmonic routing is achieved at a resonance gyration. Power flow on one graphene waveguide is switched to the other graphene waveguide by sign-reversal of the gyration. The high contrast of the plasmonic routing is preserved in the deviation of design and material parameters of the coupled graphene waveguide structure by adjusting the graphene chemical potential. Also, the gated graphene allows one to tune the operation band over a one-octave-spanning broad frequency range, keeping the contrast higher than 10^3 (99.9%). The structural and environmental robustness and the broadband tunability of the high-contrast plasmonic mod-

ulation and switchable routing have been demonstrated by analytical analysis and numerical simulations. In practice, the chemical potential and the gyration can be manipulated by controlling the gate voltage of the graphene and the external magnetic field, respectively. The intuitive analytical condition for the high-contrast plasmonic routing provides ways to allow the needed values of the chemical potential and the gyration to be in experimentally achievable ranges: $0.1 \text{ eV} < \mu_c < 1 \text{ eV}$ and $g < 0.1$. The simplicity of the considered structure, which is promising for experimental realization, is one of the important advantages of our finding. However, the simplicity of considered structure does not mean that it is trivial to realize the high-contrast plasmonic routing. It can be realized only for a resonance gyration and the corresponding graphene chemical potential satisfying the analytical condition for the high contrast, which we found in this Letter. Our findings would provide a robust and broadband tunable tool for a high-contrast plasmonic modulator, a switchable router, and for probing of ultrafast magnetization dynamics.

The data that support the findings of this Letter are available from the corresponding author upon reasonable request.

There are no conflicts of interest to declare.

-
- [1] Y. Fang and M. Sun, *Light Sci. Appl.* **4**, e294 (2015).
- [2] J. S. Schildkraut, *Appl. Opt.* **27**, 4587 (1988).
- [3] A. Melikyan, L. Alloatti, A. Muslija, D. Hillerkuss, P. C. Schindler, J. Li, R. Palmer, D. Korn, S. Muehlbrandt, D. V. Thourhout, B. Chen, R. Dinu, M. Sommer, C. Koos, M. Kohl, W. Freude, and J. Leuthold, *Nat. Photonics* **8**, 229 (2014).
- [4] C. Haffner, W. Heni, Y. Fedoryshyn, J. Niegemann, A. Melikyan, D. L. Elder, B. Baeuerle, Y. Salamin, A. Josten, U. Koch, C. Hoessbacher, F. Ducry, L. Juchli, A. Emboras, D. Hillerkuss, M. Kohl, L. R. Dalton, C. Hafner, and J. Leuthold, *Nat. Photonics* **9**, 525 (2015).
- [5] T. Nikolajsen, K. Leosson, and S. I. Bozhevolnyi, *Appl. Phys. Lett.* **85**, 5833 (2004).
- [6] J. Gosciniaik and S. I. Bozhevolnyi, *Sci. Rep.* **3**, 1803 (2013).
- [7] Z. F. Yu, G. Veronis, S. H. Fan, and M. I. Brongersma, *Appl. Phys. Lett.* **92**, 041117 (2008).
- [8] W. Cai, J. White, and M. Brongersma, *Nano Lett.* **9**, 4403 (2009).
- [9] S.-J. Im, G.-S. Ho, D.-J. Yang, Z.-H. Hao, L. Zhou, N.-C. Kim, I.-G. Kim, and Q.-Q. Wang, *Sci. Rep.* **6**, 18660 (2016).
- [10] G. Armelles, A. Cebollada, A. García-Martín, and M. U. González, *Adv. Opt. Mater.* **1**, 10 (2013).
- [11] A. V. Kimel, A. Kirilyuk, P. A. Usachev, R. V. Pisarev, A. M. Balbashov, and T. Rasing, *Nature (London)* **435**, 655 (2005).
- [12] S.-J. Im, C.-S. Ri, K.-S. Ho, and J. Herrmann, *Phys. Rev. B* **96**, 165437 (2017).
- [13] A. L. Chekhov, A. I. Stognij, T. Satoh, T. V. Murzina, O. Razdolski, and A. Stupakiewicz, *Nano Lett.* **18**, 2970 (2018).
- [14] D. O. Ignatyeva, C. S. Davies, D. A. Sylgacheva, A. Tsukamoto, H. Yoshikawa, P. O. Kapralov, A. Kirilyuk, V. I. Belotelov, and A. V. Kimel, *Nat. Commun.* **10**, 4786 (2019).
- [15] A. I. Chernov, M. A. Kozhaev, D. O. Ignatyeva, E. N. Beginin, A. V. Sadovnikov, A. A. Voronov, D. Karki, M. Levy, and V. I. Belotelov, *Nano Lett.* **20**, 5259 (2020).
- [16] V. V. Temnov, G. Armelles, U. Woggon, D. Guzatov, A. Cebollada, A. García-Martín, J. M. García-Martín, T. Thomay, A. Leitenstorfer, and R. Bratschitsch, *Nat. Photonics* **4**, 107 (2010).
- [17] V. Belotelov, L. Kreilkamp, I. Akimov, A. Kalish, D. Bykov, S. Kasture, V. Yallapragada, A. V. Gopal, A. Grishin, S. Khartsev, M. Nur-E-Alam, M. Vasiliev, L. Doskolovich, D. Yakovlev, K. Alameh, A. Zvezdin, and M. Bayer, *Nat. Commun.* **4**, 2128 (2013).
- [18] Y. S. Dadoenkova, N. N. Dadoenkova, I. L. Lyubchanskii, J. W. K. Ios, and M. Krawczyk, *IEEE Trans. Magn.* **53**, 1 (2017).
- [19] K.-S. Ho, S.-J. Im, J.-S. Pae, C.-S. Ri, Y.-H. Han, and J. Herrmann, *Sci. Rep.* **8**, 10584 (2018).
- [20] J.-S. Pae, S.-J. Im, K.-S. Ho, C.-S. Ri, S.-B. Ro, and J. Herrmann, *Phys. Rev. B* **98**, 041406(R) (2018).
- [21] D. O. Ignatyeva, D. Karki, A. A. Voronov, M. A. Kozhaev, D. M. Krichevsky, A. I. Chernov, M. Levy, and V. I. Belotelov, *Nat. Commun.* **11**, 5487 (2020).
- [22] A. A. Voronov, D. Karki, D. O. Ignatyeva, M. A. Kozhaev, M. Levy, and V. I. Belotelov, *Opt. Express* **28**, 17988 (2020).
- [23] J.-S. Pae, S.-J. Im, K.-S. Song, C.-S. Ri, K.-S. Ho, Y.-H. Han, and J. Herrmann, *Phys. Rev. B* **101**, 245420 (2020).

- [24] K.-S. Song, S.-J. Im, J.-S. Pae, C.-S. Ri, K.-S. Ho, C.-S. Kim, and Y.-H. Han, *Phys. Rev. B* **102**, 115435 (2020).
- [25] K.-S. Song, S.-J. Im, J.-S. Pae, C.-S. Ri, K.-S. Ho, and Y.-H. Han, *Appl. Phys. Lett.* **118**, 021104 (2021).
- [26] K.-S. Song, S.-J. Im, J.-S. Pae, C.-S. Ri, K.-S. Ho, and Y.-H. Han, *Phys. Rev. B* **103**, 075425 (2021).
- [27] S. A. Mikhailov and K. Ziegler, *Phys. Rev. Lett.* **99**, 016803 (2007).
- [28] P. Avouris, *IEEE J. Sel. Top. Quantum Electron* **20**, 6000112 (2014).
- [29] D. A. Kuzmin, I. V. Bychkov, and V. G. Shavrov, *Opt. Lett.* **40**, 2557 (2015).
- [30] H. Hu, X. Lin, and Y. Luo, *Prog. Electromagn. Res.* **171**, 75 (2021).
- [31] I. Smolyaninov, *Prog. Electromagn. Res.* **170**, 177 (2021).
- [32] H. Xie, Z. Wang, Y. Yang, X. Hu, H. Liu, and W. Oi, *Prog. Electromagn. Res.* **170**, 169 (2021).
- [33] V. Dal Lago, E. Suárez Morell, and L. E. F. Foa Torres, *Phys. Rev. B* **96**, 235409 (2017).
- [34] D. D. Solnyshkov, O. Bleu, and G. Malpuech, *Appl. Phys. Lett.* **112**, 031106 (2018).
- [35] D. A. Kuzmin, I. V. Bychkov, V. G. Shavrov, and V. V. Temnov, *Nanophotonics* **7**, 597 (2018).
- [36] J.-S. Pae, S.-J. Im, C.-S. Ri, K.-S. Ho, G.-S. Song, Y.-H. Han, and J. Herrmann, *Phys. Rev. B* **100**, 041405(R) (2019).
- [37] C.-S. Ri, S.-J. Im, J.-S. Pae, K.-S. Ho, Y.-H. Han, and J. Herrmann, *Phys. Rev. B* **100**, 155404 (2019).
- [38] R. V. Gorbachev, *Nat. Phys.* **8**, 896 (2012).
- [39] L. A. Ponomarenko, *Nat. Phys.* **7**, 958 (2011).
- [40] L. Britnell, *Science* **335**, 947 (2012).
- [41] Z. Wang, C. Tang, R. Sachs, Y. Barlas, and J. Shi, *Phys. Rev. Lett.* **114**, 016603 (2015).
- [42] See Supplemental Material at <http://link.aps.org/supplemental/10.1103/PhysRevB.106.L041401> for the detailed derivations of Eqs. (3) and (5)–(8).
- [43] M. Jablan, H. Buljan, and M. Soljačić, *Phys. Rev. B* **80**, 245435 (2009).
- [44] J. J. Brion, R. F. Wallis, A. Hartstein, and E. Burstein, *Phys. Rev. Lett.* **28**, 1455 (1972).